Research Paper

Chemiluminescence imaging of Duox2-derived hydrogen peroxide for longitudinal visualization of biological response to viral infection in nasal mucosa

Hyun Jik Kim[1,✉], Young Hun Seo[2], Sujin An[1], Ara Jo[1], Ick Chan Kwon[2,4], Sehoon Kim[2,3,4,✉]

1. Department of Otorhinolaryngology, Seoul National University College of Medicine, Seoul, Korea
2. Center for Theragnosis, Korea Institute of Science and Technology, Seoul, Korea
3. Division of Bio-Medical Science & Technology, KIST School, Korea University of Science and Technology (UST), Seoul 136-791, Korea
4. KU-KIST Graduate School of Converging Science and Technology, Korea University, 145, Anam-ro, Seongbuk-gu, Seoul 02841, Korea

✉ Corresponding author: sehoonkim@kist.re.kr, hyunjerry@snu.ac.kr

Abstract

Rationale: Hydrogen peroxide (H_2O_2) provides an important mechanism for resisting infectious pathogens within the respiratory tract, and accordingly, the *in situ* analysis of H_2O_2 generation in real time provides a valuable tool for assessing immune response.

Methods: In this study, we applied a chemiluminescent nanoparticle-based real-time imaging approach to noninvasive evaluation of the Duox2-mediated H_2O_2 generation after viral infection, and assessed its usefulness for analytical purposes in mouse nasal mucosa. The chemiluminescent nanoprobe employed herein (BioNT) possesses appropriate physicochemical properties, such as high sensitivity and selectivity toward H_2O_2, no background noise, deliverability to the respiratory tract, and capability of multiple injections to a single animal subject for long-term repetitive imaging.

Results: The favorable characteristics of BioNT allowed for a longitudinal study with the same mice to noninvasively evaluate the long-term evolution of endogenous H_2O_2 in the nasal epithelium after infection with influenza A virus (WS/33/H1N1). We found that nasal epithelial cells by themselves respond to viral infection by generating H_2O_2, and that the *in vivo* cumulative H_2O_2 level in the nasal mucosa peaks at day 3 post-infection. Such *in vitro* and *in vivo* temporal behaviors of the endogenous H_2O_2 generation showed a good correlation with those of Duox2 expression after infection. This correlation could be further confirmed with Duox2-deficient subjects (Duox2-knockdown NHNE cells and Duox2-knockout mutant mice) where no H_2O_2-induced chemiluminescence was detectable even after viral infection. Importantly, upon knock-down of Duox2 expression, the condition of mice caused by viral infection in the upper airway was significantly aggravated, evidencing the involvement of Duox2 in the immune defense.

Conclusion: All these results reveal a critical role of Duox2 in the infection-induced H_2O_2 production and the H_2O_2-mediated immune response to infection in the respiratory tract, well elucidating the potential of BioNT as a noninvasive tool for fundamental *in vivo* studies of infectious diseases.

Key words: hydrogen peroxide, chemiluminescence imaging, nanoprobe, Duox2, influenza A virus

Introduction

Mounting evidence suggests that reactive oxygen species (ROS) are important components of inflammation that do not only induce oxidative damage but also act as critical mediators of the host's immune response to invasive pathogens [1-3]. ROS have been regarded as one of the pathological

components of chronic inflammatory airway diseases; based on this knowledge, it has been speculated that fast clearance of ROS would be helpful to reduce lung damage [4, 5]. However, it has recently been revealed that endogenously overproduced ROS function as mediators for influencing a variety of immunological processes and eventually enhancing host immunity [6-10]. It was also reported that the modulation of ROS levels in respiratory epithelial cells is important for respiratory virus-induced innate immune mechanisms [11-13]. These controversial findings have led to growing interest in precise detection of H_2O_2 *in vivo* to assess its potential role as a target in directed therapeutics or diagnostics for oxidative stress-related diseases [14-17]. The primary chemical species of biologically generated ROS is superoxide anion $(O_2^{-}\cdot)$ that is produced by various oxidative enzymes, including nicotinamide adenine dinucleotide phosphate (NADPH) oxidase, and further converted into hydrogen peroxide (H_2O_2) to function as an important messenger molecule in various redox-dependent cellular signaling pathways. Among isoforms of NADPH oxidase, dual oxidase 2 (Duox2) has been shown to be a major one involved in the H_2O_2 generation in the respiratory tract [1-3, 18]. Interestingly, a recent work has described Duox2-generated H_2O_2 as an integral part of the host defense system at mucosal surfaces [11, 12, 18, 19], which was verified by the demonstration that a lack of Duox2-derived H_2O_2 in respiratory epithelial cells causes fatal viral infection in animal disease models [13]. According to this view, there has been growing interest in longitudinal evaluation of Duox2 activity in order to gain a better insight into the innate immunity in the respiratory tract. In this regard, optical probes that allow for timely measurement of H_2O_2 *in cellulo* as well as *in vivo* would provide a valuable tool for understanding the fundamental role of H_2O_2-producing Duox2 in immune responses.

To serve the above purpose of analyzing H_2O_2, particularly under non-invasive *in vivo* conditions, optical imaging probes are required to have (1) highly sensitive signals in the near-infrared (NIR) spectral region with maximal tissue penetration, (2) high selectivity toward H_2O_2 among other ROS, (3) deliverability to the respiratory tract upon administration in animal models, and (4) ability to accurately reflect the real-time level of H_2O_2 without interferences with earlier and later measurements during the long-term monitoring. There has been enormous recent progress in optical probes for the detection of biologically generated metabolites [20-22]. A promising candidate for H_2O_2 detection would be reaction-based small-molecule probes that are initially non-fluorescent but fluorogenic in the

NIR in response to H_2O_2 [23]. However, their application to longitudinal imaging is limited in that the fluorogenic reaction with H_2O_2 is irreversible; i.e., already-formed fluorescent products (H_2O_2-reacted probes) can no longer sense the subsequent H_2O_2 level alteration in real time, but rather stay at the reaction-occurring tissue to generate residual background signals by non-specific photoexcitation. Such residual backgrounds from the earlier imaging sessions would cause inevitable interferences with real-time information from a newly-administered probe, and would deteriorate the temporal precision. As such, it remains a challenge to develop suitable optical probes that fully meet the requirements for longitudinal imaging of H_2O_2.

Recently, a different type of optical probe has been reported that employs chemiluminescence (CL) as another promising signal modality for *in vivo* detection of H_2O_2 [24, 25]. Researchers including us have successfully applied peroxalate chemilumine-scence (POCL) to *in vivo* H_2O_2 imaging in a form of water-dispersed nanoparticles that co-incorporate all reactants needed for the H_2O_2-selective POCL generation (peroxalates and fluorescent molecules) [26-29]. Selective reaction between H_2O_2 and peroxalates produces chemical energy that is high enough to excite co-encapsulated fluorescent molecules to generate non-enzymatic light emission. Therefore, POCL is chemically generated in a highly selective manner; i.e., it does not involve background noise caused by nonspecific photoexcitation, such as tissue autofluorescence or stray excitation light, thus offering background-free signals with high sensitivity toward *in vivo* H_2O_2. Moreover, POCL is extinguished and does not glow once the energy source (peroxalates) is completely consumed after imaging. Therefore, once-extinguished CL probes would not cause any residual signal interference with newly-administered ones in the next imaging session, which is an advantage for evaluation of temporal H_2O_2 levels by repetitive imaging.

In our recent study, a highly efficient POCL nanoprobe, called "biolighted luminescent nanotorch (BioNT)", was elaborately constructed by concentra-ting the nanoparticles of a biocompatible polymeric surfactant (Pluronic F-127) with bis[3,4,6-trichloro-2-(pentyloxycarbonyl)phenyl]-oxalate (CPPO) and a 9,10-distyrylanthracene derivative (BDSA) showing solid-state fluorescence (**Figure 1**) [30]. It was shown that its high sensitivity and ultrafine colloidal structure (~15 nm in size) allowed for facile delivery to the inflamed tissues in murine models and consequent *in situ* visualization of H_2O_2 overproduced by arthritis and cancer. By taking these advantages, we here applied BioNT to the non-invasive temporal

visualization of Duox2-mediated respiratory immune responses to influenza A virus (IAV) infection. It turned out that BioNT is well-suited to imaging inflammatory H_2O_2 in the nasal mucosa *in vivo* as well as in normal human nasal epithelial (NHNE) cells *in vitro*. The resulting correlation between *in vitro* and *in vivo* infection models, as well as the good accordance with biological mechanistic studies, demonstrates that properly designed POCL nanoprobes hold great potential for unveiling the timely role of Duox2 in innate immune responses in the respiratory tract.

Methods

Viruses and reagents

Influenza A/WS/33 virus (IAV WS/33: H1N1, ATCC, Manassas, VA, USA) was used to infect NHNE cells and mouse nasal mucosa. The virus was grown in Madin-Darby canine kidney (MDCK) cells with virus growth media, according to previously published methods [31]. After a 48 h incubation at 37 °C, the supernatant was harvested and centrifuged at 323 rcf for 30 min to remove cellular debris. Viral capsids were then titrated onto MDCK cells using a tissue culture infectious dose assay, and virus stocks were stored at -80 °C. BioNT was prepared by following the literature procedure and identified by transmission electron microscopy and dynamic light-scattering measurement [30]. Anti-mouse Duox2 antibody was provided by Dr. Yun Soo Bae (Ewha Womans Univ, Seoul, Korea).

Human cell culture and mice

This study was approved by the Institutional Review Board of the Seoul National University College of Medicine (IRB number 1054-059-664) and all adult subjects who participated provided written informed consent. NHNE cell specimens were obtained from the middle nasal turbinate of five healthy volunteers. NHNE cells were then cultured using a previously published system designed for normal human nasal epithelial (NHNE) cells [2]. Briefly, NHNE cells from passage 2 (1×10^5 cells/culture) were seeded in 0.5 mL culture media on Transwell-clear culture inserts (24.5 mm; 0.45 µm pore size; Costar Co., Cambridge, MA, USA). Cells were cultured in a 1:1 mixture of basal epithelial growth media and Dulbecco's modified Eagle's media supplemented as described previously. Cells grew while submerged for the first nine days, at which point culture media was changed and then changed again every other day thereafter. An air-liquid interface (ALI) was created on day nine by removing the apical media and feeding the cultures from the basal compartment only. Culture media was changed daily after formation of the ALI. All experiments described herein used NHNE cells 14 days after ALI formation.

Male C57BL/6J (B6) mice (Orientbio, Seongnam, Korea) 7 weeks of age (19–23 g) were used as wild-type (WT), and Duox2-knockout mutant mice were purchased from The Jackson Laboratory. The recessive *thyd* mutation developed spontaneously in a B6 (129)-Duox2thyd/J mouse (Orientbio; Stock no. 005543). Duox2+/+ littermates were used as wild-type controls. All experiments were approved by the Institutional Review Board of Seoul National University College of Medicine (IRB number 2015-0263).
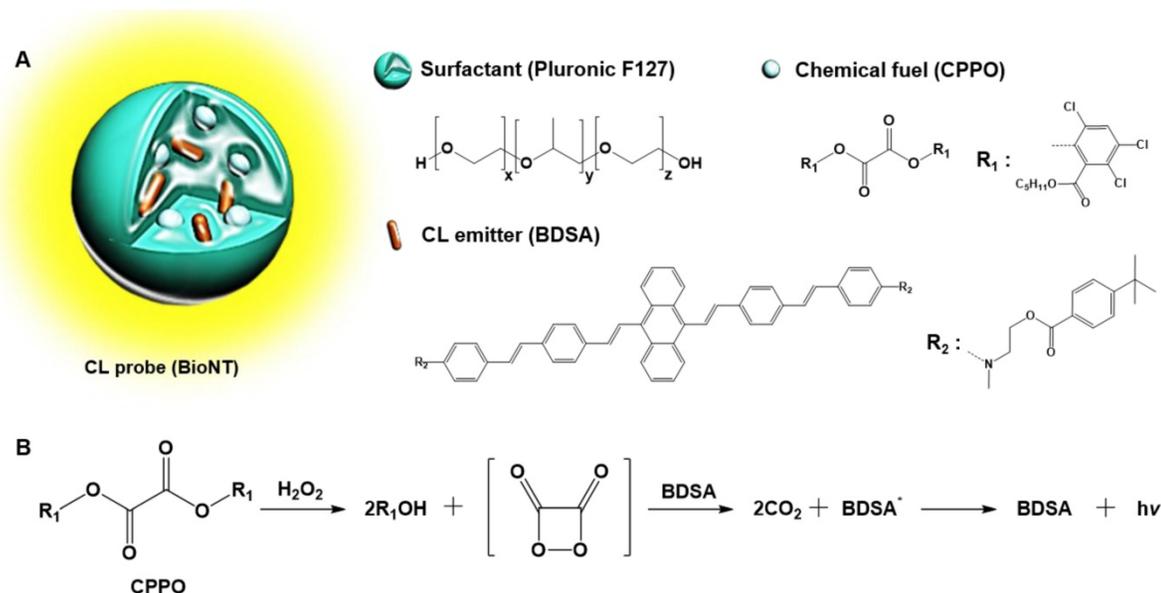
Figure 1. (A) Schematic representation and components of BioNT. **(B)** Simplified scheme of POCL reaction occurring in BioNT.

Virus inoculation

Passage 2, fully differentiated NHNE cells were either mock-infected (PBS) or inoculated with IAV (WS/33, H1N1) on the apical side of the ALI at a multiplicity of infection (MOI) of 1. After a 2 h absorption period, the inoculum was aspirated, and cells were washed twice with culture media. Culture media was then replaced and cells were incubated at 37 °C in 5% CO_2. At the designated times post-inoculation, culture supernatant was collected for virus titration using a TCID50 assay. IAV (WS/33, H1N1; 213 pfu in 30 µL PBS) was inoculated into WT or Duox2 mutant mice via intranasal delivery.

Real-time PCR

Nasal mucosa was obtained from mice infected with WS/33 (H1N1) 0, 1, 3, 5, or 7 dpi and total RNA was isolated using TRIzol (Life technology (Invitrogen Korea), Seoul, Korea). First-strand cDNA was synthesized from 3 µg of RNA using random hexamer primers and Moloney murine leukemia virus reverse transcriptase (Perkin Elmer Life Sciences, Waltham, MA, USA and Roche Applied Science, Indianapolis, IN, USA). Amplification was performed using the TaqMan Universal PCR Master Mix (PE Biosystems, Foster City, CA, USA) according to the manufacturer's protocol. Briefly, amplification reactions were completed in a total volume of 12 µL from 2 µL of cDNA template (reverse transcription mixture), oligonucleotide primers (800 nM final concentration), and TaqMan hybridization probe (200 nM). Real-time PCR probes were labeled at the 5' end with carboxyfluorescein and at the 3' end with the quencher carboxytetramethylrhodamine.

To quantify the intracellular viral level and host gene expression, cellular RNA was used to generate cDNA. The IAV level was monitored using quantitative PCR for the *PA* gene (segment 3) with the forward primer, reverse primer, and probe 5'-ggccgactacactctcgatga-3', 5'-tgtcttatggtgaatagcctgg ttt-3', and 5'-agcagggctaggatc-3', respectively. Primers for human and mouse *duox2* were purchased from Applied Biosystems (Foster City, CA, USA). Real-time PCR was performed using the PE Biosystems ABI PRISM® 7700 Sequence Detection System. Thermocycling parameters were as follows: 50 °C for 2 min, 95 °C for 10 min, and then 40 cycles of 95 °C for 15 s and 60 °C for 1 min. We quantified target mRNA levels using target-specific primer and probe sets for the IAV *PA* gene and for *duox2*. All PCR assays were quantitative and utilized plasmids containing the target gene sequences as a standard. All reactions were performed in triplicate, and all real-time PCR data were normalized to the level of the housekeeping gene glyceraldehyde phosphate dehydrogenase (GAPDH, 1×10^6 copies) to correct for variations between samples.

Plaque assay

Virus samples were serially diluted with PBS. Confluent monolayers of MDCK cells in six-well plates were washed twice with PBS and then infected in duplicate with 250 µL/well of each virus dilution. Plates were incubated at 37 °C for 45 min to facilitate virus adsorption. Following adsorption, we applied a 1% agarose overlay in complete MEM supplemented with TPCK trypsin (1 µg/mL) and 1% fetal bovine serum. Plates were incubated at 37 °C and cells were fixed with 10% formalin 2 dpi.

Cell transfection with Duox2 shRNA

Duox2 expression was suppressed using gene-specific shRNA (lentiviral particles, Santa Cruz biotechnology, Dallas, TX, USA), and we found that shRNA transfection rates were greater than 70% for NHNE cells. Cells were transfected with each shRNA using the Oligofectamine™ reagent according to the manufacturer's recommended protocol (Invitrogen, Carlsbad, CA, USA). The shRNA (10 µL, 1×10^4 infectious units of virus) and Oligofectamine™ (1 µg) were mixed individually with culture media.

In vitro and *in vivo* CL imaging

For detection of H_2O_2 production *in vitro*, infected or uninfected NHNE cells were seeded into cell culture Transwell-Clear inserts. After washing twice with PBS (pH 7.4) to remove trace amounts of growth media or supernatant, NHNE cells were incubated in PBS (300 µL) containing BioNT dispersion (6.6 mg) for 120 min, and then subjected to the CL intensity measurement by imaging. *In vivo* imaging of infected or uninfected mice was done under anaesthesia at designated time points after intranasal administration of BioNT (40 µL, 0.88 mg/mL). Both *in vitro* and *in vivo* CL imaging experiments were done with an IVIS Spectrum imaging system (Caliper, USA) and the CL intensities were measured as a radiance value from the regions of interest designated in the obtained images (**Figure S1-2**).

Statistical analyses

At least three independent replicate experiments were performed with cultured cells from each donor, and the results are presented as the mean value ± standard deviation (SD) based on triplicate measurements. For *in vivo* conditions, CL intensities, real-time PCR and plaque assay results are presented as the mean ± standard deviation (SD) based on measurements from five individual mice. Significant differences between control and infection groups

were assessed using analysis of variance (ANOVA) with a *post hoc* test. All statistical analysis was conducted using Graphpad Prism software (version 5; Graphpad Software, La Jolla, CA, USA) and p-values less than 0.05 were considered statistically significant.

Results

In vitro CL imaging of IAV infection-induced H_2O_2 generation

The enhanced CL emission from BioNT is of practical utility in that it might allow for high-sensitivity H_2O_2 detection *in vivo* as well as *in vitro* down to the range of 10^{-7} M (**Figure S3**). To assess whether BioNT can indeed generate CL emission in cells in response to H_2O_2, NHNE cells pretreated with exogenous H_2O_2 (250 µM) were inoculated with BioNT (6.6 mg/300 µL PBS), and then *in vitro* CL signals were measured by imaging. Results showed that BioNT generates a detectable CL signal under the given *in vitro* condition, which is initially intense but gradually decays to complete extinction 30

min after treatment (**Figure S4**), demonstrating the characteristic peroxalate-consuming behavior of a POCL probe.

We next sought to evaluate whether BioNT is indeed capable of detecting endogenous H_2O_2 produced in NHNE cells by IAV infection. To see the initial cellular response to infection, NHNE cells were treated with IAV WS/33 (H1N1) at a MOI of 1, and the temporal CL signals from the cell-stained BioNT were measured by imaging. As shown in **Figure 2A**, the CL emission was silent immediately after IAV infection, but the contrast to the negative control began to increase at ~40 min post-infection to reach the maximum value at 60 min. Thereafter, the signal faded out to complete extinction at 90 min. The maximum radiance value is about an order of magnitude lower than that observed above with exogenous H_2O_2 at 250 µM (**Figure S4**), implying that the concentration of endogenously generated H_2O_2 by IAV infection under the given condition is far lower than 250 µM. Importantly, the intense CL response to IAV infection at 60 min was significantly reversed in
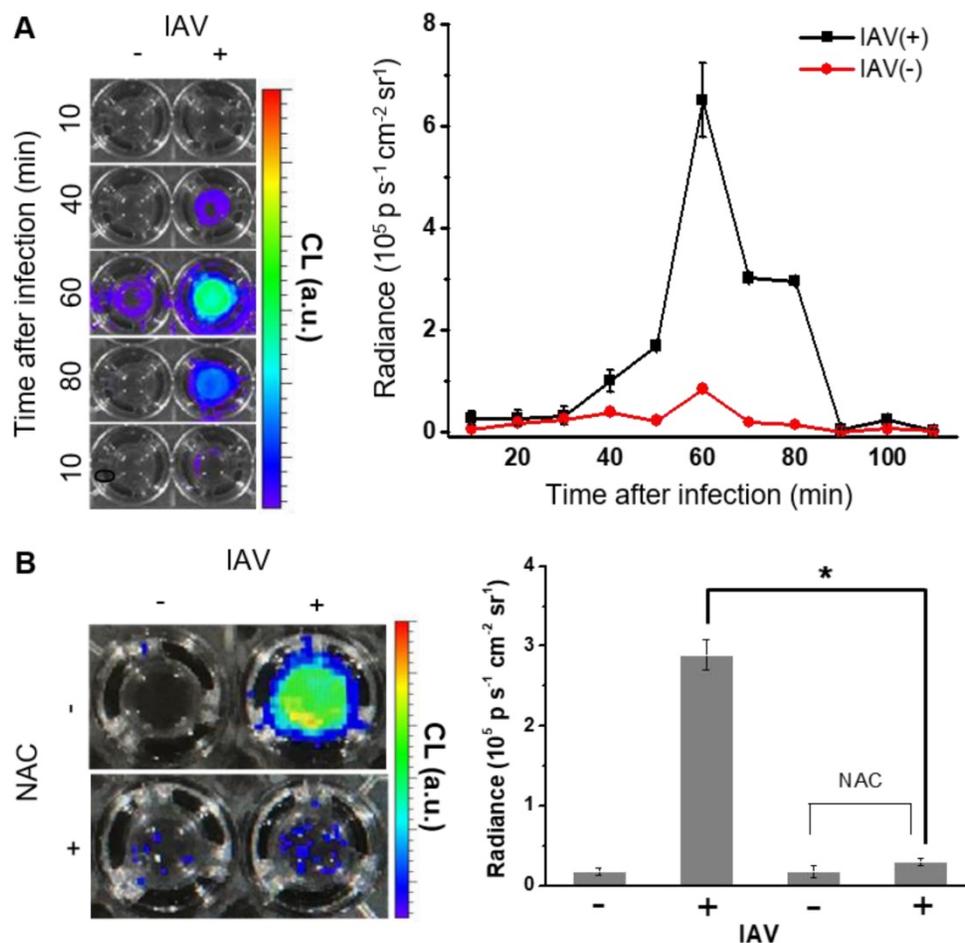
Figure 2. (A) CL images of BioNT (6.6 mg/300 µL PBS) in NHNE cells that were infected with IAV WS/33 (H1N1) at a MOI of 1 or uninfected (left), and the corresponding temporal evolution of the CL intensities (right). Time points post-infection are indicated. **(B)** CL images (left) and the corresponding CL intensities (right) of BioNT in NHNE cells, taken at 60 min post-infection with or without pretreatment with ROS-scavenging antioxidant NAC (10 µM) 1 h prior to infection. Results are presented as the mean ± standard deviation (*: $p < 0.05$ when compared to mock-infected cells, n=5).

cells that were pretreated with an ROS-scavenging antioxidant, *N*-acetylcysteine (NAC, 10 μM), 1 h prior to infection (**Figure 2B**). These results confirm that the CL generation upon IAV infection is attributed to the endogenously produced H_2O_2 by the infected cells. It is further speculated that there is an induction period (~40 min) in the cellular response to produce detectable H_2O_2 after infection.
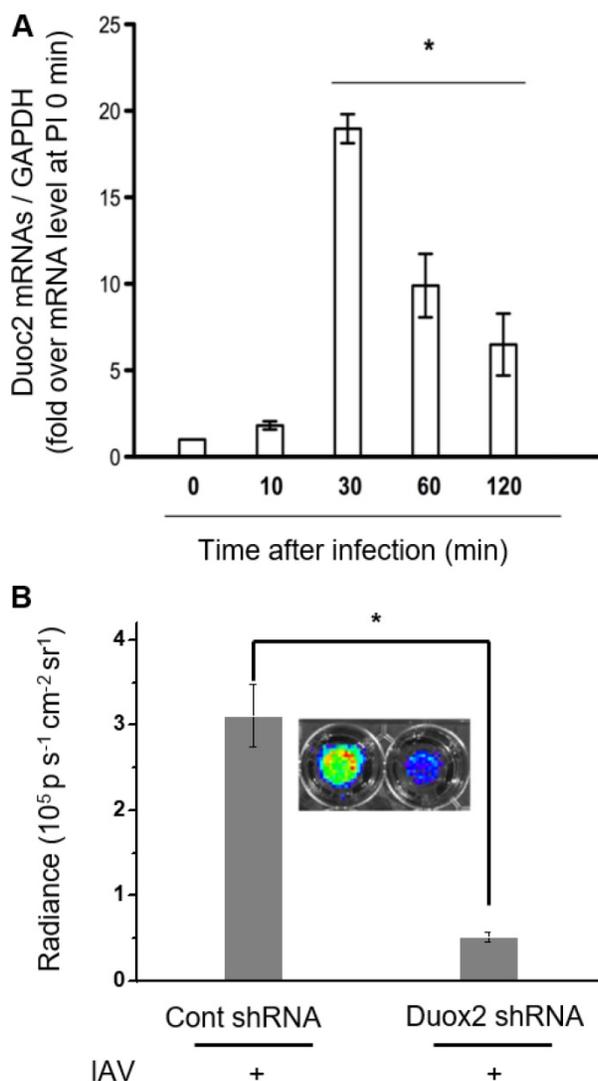
Figure 3. (A) Real-time PCR monitoring of *Duox2* mRNA level in NHNE cells at time points post-infection with IAV WS/33 (H1N1) at a MOI of 1. Results are presented as the mean ± standard deviation (*: $p < 0.05$ when compared with mock-infected cells, n=5). **(B)** CL images (inset) and the corresponding CL intensities of BioNT in NHNE cells (60 min post-infection) transfected with control shRNA or Duox2-specific shRNA. CL intensities are presented as the mean ± standard deviation (*: $p < 0.05$, n=5).

Correlation between infection-induced H_2O_2 generation and Duox2 expression

In our previous report, it turned out that Duox2 is highly expressed by IAV infection, being a critical part of the interferon-related antiviral innate immune response in NHNE cells [12]. According to this finding, Duox2 is speculated as a possible Nox subtype that might be involved in H_2O_2-responsive CL enhancement after IAV infection in NHNE cells. To verify this, cells were infected with IAV WS/33 (H1N1) at a MOI of 1, and then cellular mRNA levels for Duox2 were measured using real-time PCR. It was observed that the mRNA level of Duox2 began to increase at 10 min post-infection and reached a maximum at 30 min (18.4 ± 0.7-fold over the initial value, p<0.05; **Figure 3A**). Protein expression of Duox2 was also elevated from 10 min after infection, and the highest expression was observed at 30 min in NHNE cells infected under the same condition (**Figure S5A**). To our interest, the observed temporal pattern of Duox2 transcriptional changes in the infected NHNE cells is well accordant with that of the IAV-induced CL signals in **Figure 2A**, in spite of the time difference between them. The delayed CL emission compared to Duox2 expression is attributable to time-consuming steps that are required after transcription and translation in the Duox2 maturation for H_2O_2 generation (for example, traveling to the apical cell membrane and glycosylation to adopt the active form) [2].

To further determine whether Duox2 is indeed involved in intracellular H_2O_2 generation by IAV infection, we compared CL intensities of BioNT between NHNE cells with and without knock-down of Duox2 gene expression. To this end, NHNE cells were transfected with Duox2 shRNA or control shRNA, respectively, and then subjected to IAV infection. It was found that cell treatment with Duox2 shRNA decreased the endogenous *Duox2* gene expression by 78% compared to the control shRNA transfection. Coinciding with Duox2 silencing, the CL intensity of BIoNT was also reduced by 83% (**Figure 3B**), indicating that the infection-induced production of H_2O_2 was significantly diminished. All these results suggest that Duox2 may constitute a critical part of the H_2O_2 generation pathway in the virus-infected nasal epithelium.

In vivo CL imaging of IAV-infected mouse nasal mucosa

We next performed *in vivo* CL imaging of endogenous H_2O_2 produced in nasal mucosa, to evaluate the diagnostic potential of BioNT for early-stage infection. Prior to this, we repeated *in vivo* imaging with exogenous H_2O_2 by administering fresh BioNT to the same mouse once a day for up to 5 days. In each daily imaging session, it was reliably observed that the CL emission reaches a maximum at 5 min after BioNT inoculation and then decreases to a hardly detectable level at 240 min (**Figure S6**). Such a typical temporal CL pattern that is reliably repeatable

in each imaging session with newly-administered BioNT, along with the experimentally observed colloidal stability (**Figure S7**), suggests that the CL-emitting nanostructure of BioNT is stably maintained upon inoculation in the nasal mucosal condition and thus applicable to diagnostic *in vivo* imaging of H_2O_2. Moreover, complete CL extinction to the initial blank level in every 24 h post-inoculation (**Figure S6**) allows for next-session CL imaging with no signal interference. By virtue of these combined merits, BioNT could allow multiple sessions of CL imaging in the same mouse for long-term tracing of *in vivo* H_2O_2 level variation after viral infection. To demonstrate this, B6 mice were infected with IAV WS/33 (H1N1) via intranasal administration (213 pfu/30 µL), and then BioNT (0.88 mg/40 µL) was intranasally inoculated 0, 1, 3, 5, 7 days post-infection (dpi) for CL imaging. As represented in **Figure 4A**, each *in vivo* CL imaging session showed the typical luminescing behavior of BioNT, where the CL emission from the infected nasal mucosa was the strongest at 5 min after BioNT inoculation and then faded out. **Figure 4B** shows the result of multiple-session CL imaging at the selected dpi, where the images at each session were taken 5 min

post-inoculation of BioNT. Compared to the non-infected control group, the infected mice presented distinctly measurable CL emission from 1 dpi. Multiple-session imaging revealed that the intensity of H_2O_2-responsive CL emission increases abruptly at 3 dpi and then gradually decreases to extinction at 7 dpi, noninvasively reflecting the long-term evolution of *in vivo* H_2O_2 level in the infected nasal mucosa.

To validate the role of Duox2 in acute IAV infection *in vivo*, the levels of *Duox2* mRNA and Duox2 protein expression in the infected nasal mucosa were determined by real-time PCR and western blot analysis, respectively, at 0, 1, 3, 5, and 7 dpi. As shown in **Figure 5A** and **Figure S5B**, the *Duox2* mRNA level and protein expression in the infected wild-type (WT) B6 mice evolved similarly to the temporal pattern of multiple-session CL imaging (**Figure 4B**) with an abrupt increase at 3 dpi (mRNA level: 6.82 ± 2.3-fold over mean mRNA level of control mice, $p < 0.05$) and a gradual decrease thereafter. To further confirm the role of Duox2, we compared the H_2O_2-responsive CL intensities of BioNT applied to the infected nasal mucosa between WT and Duox2-knockout mutant mice (Duox2[thyd/thyd]; **Figure**
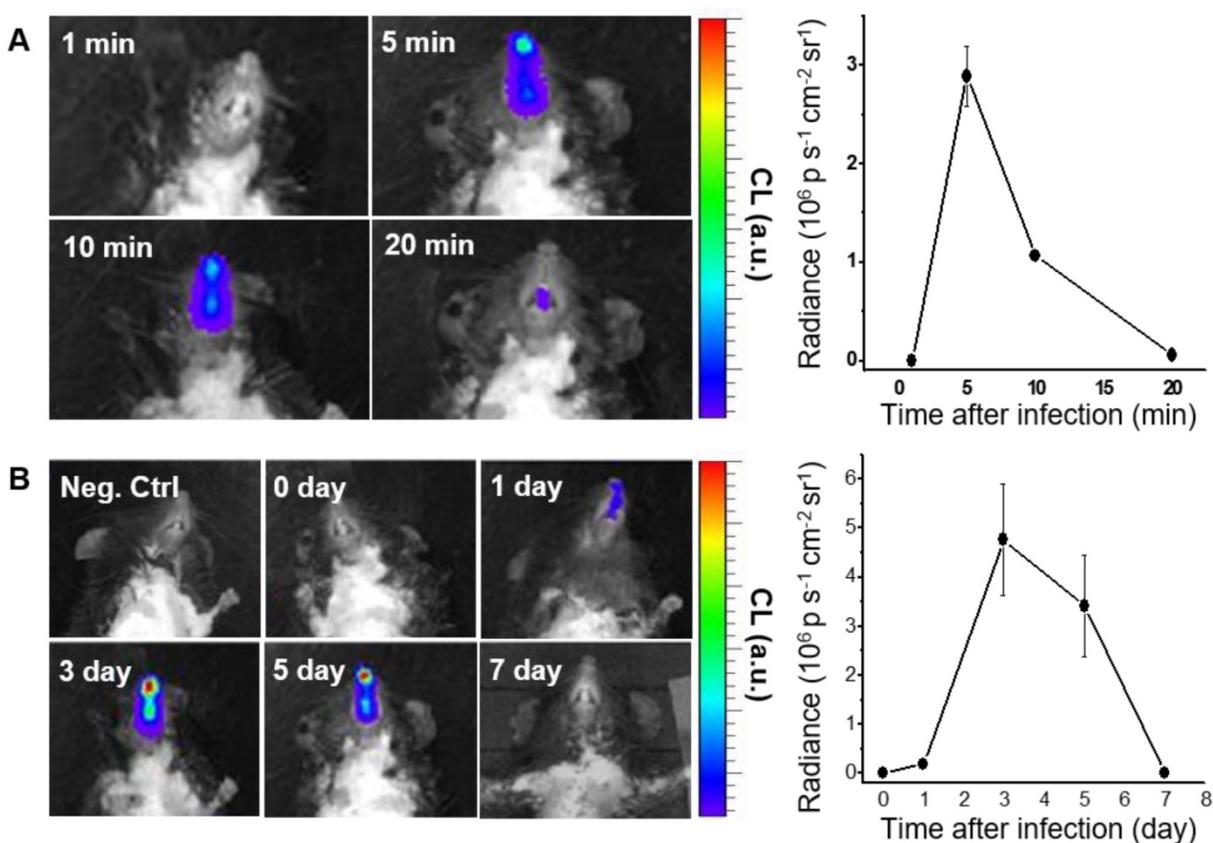
Figure 4. CL imaging of WT mice infected with IAV WS/33 (H1N1) in the nasal mucosa (*n*=5). **(A)** Representative CL images (left) and the corresponding CL intensities (right) of a single imaging session, taken 3 days post-infection (dpi). Imaging time points (min) post-inoculation of BioNT are indicated. **(B)** CL images (left) and the corresponding CL intensities (right) of multiple imaging sessions, taken 0, 1, 3, 5 and 7 dpi. Each image was taken 5 min post-inoculation of BioNT. Results are presented as the mean ± standard deviation (*: $p < 0.05$ when compared to the same mice at 0 dpi).

5B). Upon imaging at 3 dpi, intense CL emission was observed in the infected WT mice, as seen in **Figure 4B**. In sharp contrast, Duox2-deficient mutant mice showed no discernable CL contrast even after viral infection, evidencing that Duox2 is indeed involved in the infection-induced H_2O_2 production in nasal mucosa.
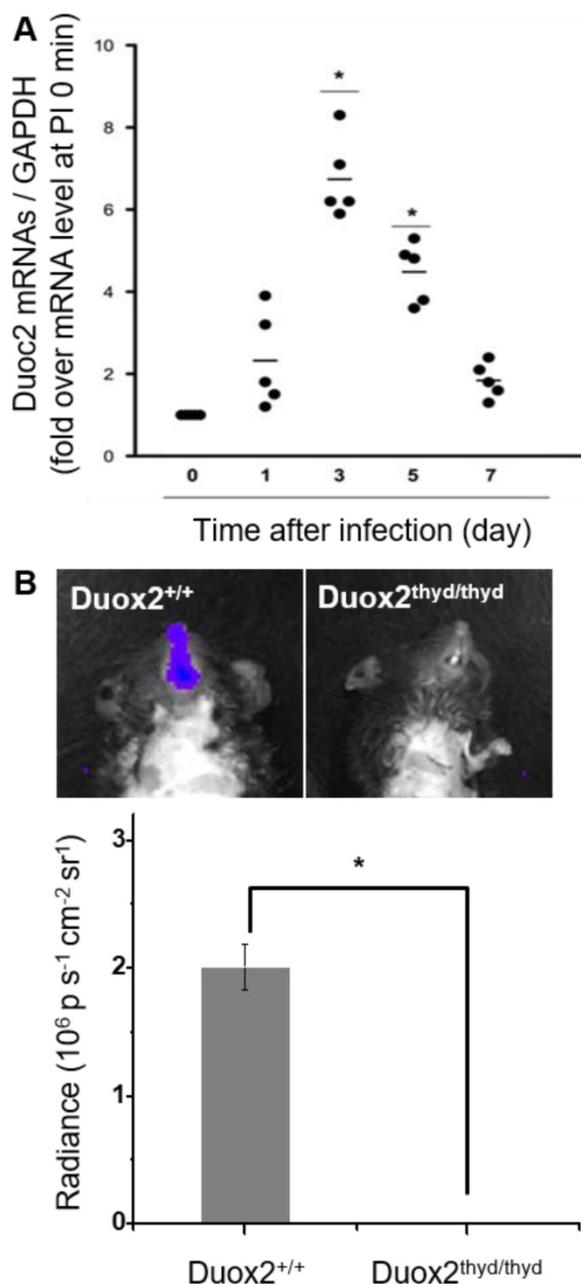
Figure 5. (A) Real-time PCR monitoring of *Duox2* mRNA level in the nasal mucosa of WT mice (*n*=5) at the indicated time points after infection (dpi) with 213 pfu IAV WS/33 (H1N1). Results are presented as the mean values (*: p<0.05 when compared to the same mice at 0 dpi). **(B)** CL images (left) and the corresponding CL intensities (right) of BioNT in the nasal mucosa of WT mice (Duox2^+/+) and Duox2-knockout mutant mice (Duox2^thyd/thyd), both of which were infected with 213 pfu IAV WS/33 (H1N1). CL imaging was performed at 3 dpi and CL intensities are presented as the mean ± standard deviation (*: *p* < 0.05, *n*=5).

It was also revealed that, compared to WT mice, the survival rate after IAV infection is significantly

low in the Duox2-knockout mutant group to such an extent that Duox2-deficient mice survived no more than 10 dpi (**Figure 6A**). When examined at 7 dpi, IAV-infected Duox2-knockout mice showed considerably higher IAV mRNA levels than WT mice (**Figure 6B**) in conjunction with a similarly higher viral titer in nasal lavage (NAL) fluid (Duox2-knockout mutant mice 3.4×10^4 versus WT mice 1.2×10^4; **Figure 6C**). These results are well correlated with the temporal regulation of *in vivo* H_2O_2 visualized by the CL imaging with BioNT, evidently unraveling the central role of Duox2 in an innate antiviral immune response.

Discussion

This study demonstrates that a highly efficient POCL nanoprobe (BioNT) can be applied to sensitive temporal visualization of innate immune response to viral infection in both nasal epithelial cells *in vitro* and nasal mucosa *in vivo*. Our results of CL imaging with BioNT clearly revealed that the endogenous H_2O_2 level was dramatically raised in response to IAV infection in nasal epithelial cells *in vitro* as well as nasal mucosa *in vivo*, well envisaging the temporal Duox2 activity evolution.

In this study, we employed chemiluminescent BioNT as an *in vivo* measuring tool that is highly sensitive and selective toward H_2O_2, free from background noise, and capable of multiple injection to a single animal subject for long-term repetitive imaging. We demonstrated that such characteristics of BioNT are a good fit for a longitudinal study to noninvasively evaluate the temporal variation of endogenous H_2O_2 in the nasal epithelium of each mouse infected with IAV. *In vitro* imaging with BioNT revealed that NHNE cells respond by themselves to IAV virus and begin to overproduce intracellular H_2O_2 at ~40 min post-infection. On an *in vivo* animal level, multiple-session chemiluminescence imaging with repetitive injection of BioNT successfully visualized a long-term response of the respiratory mucosa to viral infection; the IAV-induced H_2O_2 production in the nasal mucosa was observed to reach a maximum level at day 3 after infection and IAV-induced CL signals were not detected at day 7. From the current results, we estimate that significantly localized visualization of CL imaging is possible by using BioNT in nasal mucosa of IAV-infected mice and the multi-molecule integrated nanostructures can be stably maintained in the nasal mucosal condition. This localized H_2O_2 imaging from BioNT would provide an opportunity for the non-invasive detection of Duox2-related antiviral immune response or assessment of the severity of damage from viral infection on respiratory mucosa.
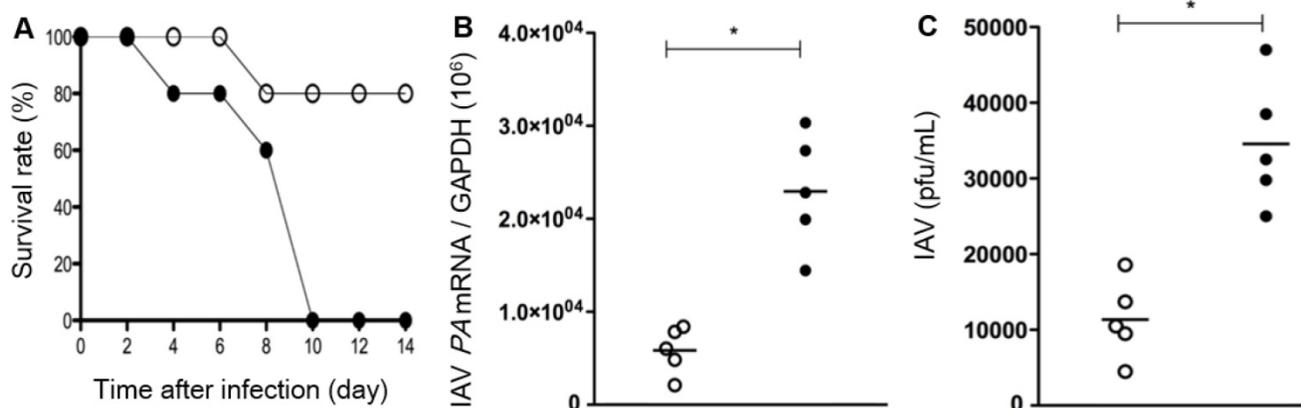
Figure 6. Survival rates **(A)**, IAV mRNA levels in the lung tissues **(B)**, and the viral titer result in BAL fluid **(C)** of WT mice (Duox2$^{+/+}$, open circles) and Duox2-knockout mutant mice (Duox2$^{thyd/thyd}$, closed circles), both of which were infected with IAV under the same condition. Results are presented as the mean values from five independent mice (*, p<0.05 compared to the levels with WT mice). All the results elucidate that the H$_2$O$_2$-producing Duox2 is an essential component in nasal mucosa to resist the viral infection.

In order to discern that Duox2 is primarily involved in immunity and H$_2$O$_2$ production in the respiratory tract, we manipulated the *Duox2* gene and evaluated the responses against IAV infection in mouse nasal mucosa. Upon knock-down of Duox2 expression, the condition caused by IAV-induced acute infection in the upper airway was significantly aggravated, affirming the critical role of Duox2 in the immune defense. We further attempted to correlate the Duox2 activity with the temporal evolution of IAV-induced H$_2$O$_2$ obtained by imaging with BioNT. Indeed, we found a good correlation between the Duox2 activity and H$_2$O$_2$-induced CL signals in that the CL signals from the infected cells *in vitro* and nasal mucosa *in vivo* were the most intense at the time points when Duox2 transcription is the most significantly increased after viral infection in each case. Moreover, IAV-induced CL signals were no more detectable in Duox2-deficient subjects, i.e., NHNE cells that were transfected with Duox2-silencing shRNA, and the nasal mucosa of Duox2-knockout mutant mice. These findings strongly suggested that Duox2 in the nasal epithelial cell is indeed involved in the infection-induced H$_2$O$_2$ production in the nasal mucosa, and in turn plays a crucial role in the H$_2$O$_2$-mediated immune response to IAV in the respiratory tract.

Summary

We have demonstrated that a highly sensitive chemiluminescent nanoprobe with appropriate physicochemical properties (BioNT) enables longitudinal, noninvasive, visual quantification of H$_2$O$_2$ that is associated with IAV infection-caused immune responses in nasal mucosa. The H$_2$O$_2$-specific BioNT signaling patterns in IAV-infected NHNE cells *in vitro* and nasal mucosa *in vivo*, along with its correlation with the temporal Duox2 activity, unraveled the biological role of Duox2 in the immune defense against viral infection to the respiratory tract, well elucidating the potential of BioNT as a useful imaging agent to predict mucosal immunity in respiratory mucosa.

Abbreviations

ALI: air-liquid interface; BioNT: biolighted luminescent nanotorch; CL: chemiluminescence; CPPO: bis[3,4,6-trichloro-2-(pentyloxycarbonyl)phenyl]-oxalate; Duox2: dual oxidase 2; H$_2$O$_2$: hydrogen peroxide; IAV: influenza A virus; MDCK: madin-darby canine kidney; MOI: multiplicity of infection; NAC: *n*-acetylcysteine; NADPH: nicotinamide adenine dinucleotide phosphate; NHNE: normal human nasal epithelial; NIR: near-infrared; O$_2^{-\cdot}$: superoxide anion; POCL: peroxalate chemiluminescence; ROS: reactive oxygen species.

Acknowledgements

Supplementary Material

Supplementary figures.
http://www.thno.org/v08p1798s1.pdf

Competing Interests

The authors have declared that no competing interest exists.

References

[1] van der Vliet A. NADPH oxidases in lung biology and pathology: Host defense enzymes, and more. Free Radic Biol Med. 2008; 44: 938-55.

[2] Kim HJ, Kim CH, Ryu JH, Kim MJ, Park CY, Lee JM, et al. Reactive oxygen species induce antiviral innate immune response through IFN-λ regulation in human nasal epithelial cells. Am J Respir Cell Mol Biol. 2013; 49: 855-65.

[3] Mellqvist UH, Hansson M, Brune M, Dahlgren C, Hermodsson S, Hellstrand K. Natural killer cell dysfunction and apoptosis induced by chronic myelogenous leukemia cells: Role of reactive oxygen species and regulation by histiamine. Blood. 1999; 65: 196-204.

[4] Barnes PJ, Shapiro SD, Pauwels RA. Chronic obstructive pulmonary disease: molecular and cellular mechanisms. Eur Respir J. 2003; 22: 672-688.

[5] Rahman I. Oxidative stress, chromatin remodeling and gene transcription in inflammation and chronic lung disease. J Biochem Mol Biol. 2003; 36: 95-109.

[6] Mahadev K, Motoshima H, Wu X, Ruddy JM, Arnold RS, Cheng G, et al. The NAD(P)H oxidase homolog Nox4 modulates insulin-stimulated generation of H_2O_2 and plays an integral role in insulin signal transduction. Mol Cell Biol. 2004; 24: 1844-54.

[7] Lambeth JD, Kawahara T, Diebold B. Regulation of Nox and Duox enzymatic activity and expression. Free Radic Biol Med. 2007; 43: 319-31.

[8] Schwarzer C, Marchen TE, Illek B, Fischer H. NADPH oxidase-dependent acid production in airway epithelial cells. J Biol Chem. 2004; 279: 36454-61.

[9] Ris-stalpers C. Physiology and Pathophysiology of the DUOXes. Antioxid Redox Signal. 2006; 8: 1563-72.

[10] Weichart D, Gobom J, Klopfleisch S, Häsler R, Gustavsson N, Billmann S, et al. Analysis of NOD2-mediated proteome response to muramyl dipeptide in HEK293 cells. J Biol Chem. 2006; 281: 2380-9.

[11] Hong SN, Kim JY, Kim H, Kim DY, Won TB, Han DH, et al. Duox2 is required for the transcription of pattern recognition receptors in acute viral lung infection: An interferon-independent regulatory mechanism. Antiviral Res. 2016; 134: 1-5.

[12] Kim HJ, Kim CH, Kim MJ, Ryu JH, Seong SY, Kim S, et al. The Induction of Pattern-Recognition Receptor Expression against Influenza A Virus through Duox2-Derived Reactive Oxygen Species in Nasal Mucosa. Am J Respir Cell Mol Biol. 2015; 53: 525-35.

[13] Strengert M, Jennings R, Davanture S, Hayes P, Gabriel G, Knaus UG. Mucosal reactive oxygen species are required for antiviral response: role of Duox in influenza a virus infection. Antioxid Redox Signal. 2014; 20: 2695-709.

[14] Tal MC, Sasai M, Lee HK, Yordy B, Shadel GS, Iwasaki A. Absence of autophagy results in reactive oxygen species-dependent amplification of RLR signaling. Proc Natl Acad Sci U S A. 2009; 106: 2770-5.

[15] Soucy-Faulkner A, Mukawera E, Fink K, Martel A, Jouan L, Nzengue Y, et al. Requirement of NOX2 and Reactive Oxygen Species for Efficient RIG-I-Mediated Antiviral Response through Regulation of MAVS Expression. PLoS Pathog. 2010; 6: e1000930.

[16] Weinstain R, Savariar EN, Felsen CN, Tsien RY. In vivo Targeting of Hydrogen Peroxide by Activatable Cell-Penetrating Peptides. J Am Chem Soc. 2014; 136: 874-7.

[17] Fang J, Seki T, Maeda H. Therapeutic strategies by modulating oxygen stress in cancer and inflammation. Adv Drug Deliv Rev. 2009; 61: 290-302.

[18] Liu T, Castro S, Brasier AR, Jamaluddin M, Garofalo RP, Casola A. Reactive Oxygen Species Mediate Virus-induced STAT Activation. J Biol Chem. 2004; 23: 2461-9.

[19] Lipinski S, Till A, Sina C, Arlt A, Grasberger H, Schreiber S, et al. DUOX2-derived reactive oxygen species are effectors of NOD2-mediated antibacterial responses. J Cell Sci. 2009; 122: 3522-30.

[20] Kim JY, Sahu S, Yau YH, Wang X, Shochat SG, Nielsen PH, et al. Detection of Pathogenic Biofilms with Bacterial Amyloid Targeting Fluorescent Probe, CDy11. J Am Chem Soc. 2016; 138: 402-7

[21] Liu C, Yang C, Lu L, Wang W, Tan W, Leung CH, et al. Luminescent iridium(III) complexes as COX-2-specific imaging agents in cancer cells. Chem Comm. 2017; 53: 2822-5

[22] Metelev V, Zhang S, Zheng S, Kumar ATN, Bogdanov A Jr. Fluorocarbons Enhance Intracellular Delivery of Short STAT3-sensors and Enable Specific Imaging. Theranostics. 2017; 7: 3354-68

[23] Guo Z, Park S, Yoon J, Shin I. Recent progress in the development of near-infrared fluorescent probes for bioimaging applications. Chem Soc Rev. 2014; 43: 16-29.

[24] Dong B, Song X, Kong X, Wang C, Tang Y, Liu Y, et al. Simultaneous Near-Infrared and Two-Photon In Vivo Imaging of H_2O_2 Using a Ratiometric Fluorescent Probe based on the Unique Oxidative Rearrangement of Oxonium. Adv Mater. 2016; 28: 8755-9.

[25] Ren M, Deng B, Zhou K, Kong X, Wang JY, Lin W. Single Fluorescent Probe for Dual-Imaging Viscosity and H_2O_2 in Mitochondria with Different Fluorescence Signals in Living Cells. Anal Chem. 2017; 89: 552-5.

[26] Lee D, Khaja S, Velasquez-Castano JC, Dasari M, Sun C, Petros J, et al. In vivo imaging of hydrogen peroxide with chemiluminescent nanoparticles. Nat Mater. 2007; 6: 765-9.

[27] Lee YD, Lim CK, Singh A, Koh J, Kim J, Kwon IC, et al. Dye/Peroxalate Aggregated Nanoparticles with Enhanced and Tunable Chemiluminescence for Biomedical Imaging of Hydrogen Peroxide. ACS Nano. 2012; 6: 6759-66.

[28] Zhen X, Zhang C, Xie C, Miao Q, Lim KL, Pu K. Intraparticle Energy Level Alignment of Semiconducting Polymer Nanoparticles to Amplify Chemiluminescence for Ultrasensitive iIn Vivo Imaging of Reactive Oxygen Species. ACS Nano. 2016; 10: 6400-9.

[29] Shuhendler AJ, Pu K, Cui L, Uetrecht JP, Rao J. Real-time imaging of oxidative and nitrosative stress in the liver of live animals for drug-toxicity testing. Nat Biotechnol. 2014; 32: 373-80.

[30] Singh A, Seo YH, Lim CK, Koh J, Jang WD, Kwon IC, et al. Biolighted Nanotorch Capable of Systemic Self-Delivery and Diagnostic Imaging. ACS Nano. 2015; 9: 9906-11.

[31] Wang J, Oberley-Deegan R, Wang S, Nikrad M, Funk CJ, Hartshorn KL, Mason RJ. Differentiated human alveolar type II cells secrete antiviral IL-29 (IFN-lambda 1) in response to influenza A infection. J Immunol. 2009; 182: 1296-1304.